UNIVERSITY OF NOVA GORICA
GRADUATE SCHOOL

Meshless modeling of thermo-mechanics of low-frequency electromagnetic direct chill casting

DISSERTATION

Boštjan Mavrič

Mentor: Prof. Dr. Božidar Šarler

Nova Gorica, 2017

UNIVERZA V NOVI GORICI
FAKULTETA ZA PODIPLOMSKI ŠTUDIJ

Brezmrežno modeliranje termomehanike nizkofrekvenčnega elektromagnetnega polkontinuirnega ulivanja

DISERTACIJA

Boštjan Mavrič

Mentor: prof. dr. Božidar Šarler

Nova Gorica, 2017

Meshless modeling of thermo-mechanics of low-frequency electromagnetic direct chill casting

Abstract

The aim of this dissertation is to devise a meshless model describing the thermomechanical phenomena, which occur during DC casting of aluminium alloys under the influence of electromagnetic stirring. The thermoemchanical phenomena are important, because they can cause several type of defects, which can significantly deteriorate the quality of the resulting billet. The two most important of them are the hot tearing, which causes cracks to appear in the mushy zone, and the porosity, which demonstrates itself as micrometer sized voids in the microstructure of the billet.

To calculate the stresses and strains, a computational model, stated in axial symmetry is formulated. It describes the stationary state of the casting process stated in Eulerian formulation by fixing the computational domain to the mold of the casting device allowing the material to move through the computational domain. The stresses are calculated from the stress equilibrium equations. Small strain approximation is used to consider three contributions to strain. The strain consists of the thermal strain, which is caused by the inhomogeneous thermal profile in the billet, the viscoplastic strain caused by the irreversible deformation because of the large stresses occurring in the billet and the elastic strain.

The spatial discretization of the governing equations is performed by local radial basis function collocation method (LRBFCM) and the temporal discretization is achieved by the method of lines with implicit Euler formula. The method used for spatial discretization uses radial basis functions augmented by monomials to approximate the solution values on localized stencils. This approximation is used to construct the discretization coefficients of the differential operators present in the model. A flexible framework for formulation of multiphysics problems was developed to use obtained discretization coefficents to construct the temporal discretization of the

governing equations.

The performance of the method was tested on several benchmark test cases. The accuracy of the discretization was estimated by comparing analytical and numerical solution of several stationary problems in thermomechancis. Of special interest was performance of the method with respect to the choice of the shape parameter, which determines the spatial scale of the radial basis functions. Besides this, the dependence of the condition number of the interpolation matrix on the shape parameter was studied. The condition number was found fit to replace the condition number as shape-determining free parameter of the method.

The implementation of the solver of time dependent problems was tested on problem of thermoelasticity, which couples the thermal transport with elastic waves. The results of the problem were compared with the finite element method, showing comparable results. The results were also compared with the results obtained by meshless local Petrov-Galerkin method and the proposed local collocation method demonstrated significantly better solution quality in the studied case.

The performance of the solver used to solve the system of nonlinear equations given by the viscoplastic constitutive equations was estimated on a quasi zero-dimensional problem. The results matched perfectly. Solution of a more complicated problem was obtained with the proposed method and FEM, both methods giving practically the same solution, although some serious limitations of the chosen FEM solver became evident during the selection of the problem parameters.

Finally, the devised method was applied to the problem of DC casting of aluminium alloys. The thermomechanical model relies on a model of heat and mass transfer to obtain the input fields needed in the solver. The required fields are: temperature, pressure, liquid fraction and electromagnetic force. The thermomechnics model performs calculations only in the mechanically coherent part of the mushy zone, below the coherency isotherm. The model iteratively determines the boundary conditions on the contact between the billet and the mold. After the solution of the thermomechanical model reaches stationary state, the obtained results are used to determine the hot tearing susceptibility.

The dependence of the hot tearing susceptibility on various casting parameters is estimated. The model successfully reproduces the lambda curve, which is typical for dependence of the hot tearing on the percentage of the alloying element.

The selected spatial discretization method is found to be capable of modeling the thermomechanical problems associated with DC casting of aluminium alloys. It is demonstrated to be capable of solving partial differential equations on irregular meshes with same performance as if the regular grids were used. The impact of the augmentation monomials on the behavior of the method is investigated, suggesting the requirement to use augmentation with linear polynomial to increase the method reliability.

The developed model of thermomechanics during DC casting, tightly coupling the fluid flow, electromagnetic field and heat transfer to viscoplasticity can model the influence of different casting parameters on the formation of some mechanical defects which occur during the process of DC casting.

Keywords meshelss methods, thermomechanics, viscoplasticity, radial basis functions, local collocation method, shape parameter, direct-chill casting, hot tearing, porosity, aluminium alloys, electromagnetic casting

Brezmrežno modeliranje termomehanike nizkofrekvenčnega elektromagnetnega polkontinuirnega ulivanja

Povzetek

Namen te disertacije je razvoj brezmrećnega modela termomehanskih pojavov, ki so prisotni med DC ulivanjem aluminiujevih zlitin pod vplivom elektromagnetnega mešanja. Ti pojavi so pomembni, ker lahko povzročijo več vrst defektov, ki lahko bitveno poslabšajo kvaliteto ulitega droga. Med njimi sta najpomembnejša vroče trganje, ki povzroči pojavljanje razpok v kašastem področju, in poroznost, ki se kaže kot prisotnost mikrometerskih praznin v notranjosti droga.

Za izračun napetosti in deformacij je bil razvit osnosimetrični računski model. Z Eulerjevim opisom modelira stacionarno stanje med procesom litja. Računska domena je pripeta na kokilo, skoznjo pa se premika strjeni material. Za izračun napetosti se rešuje ravnovesna enačba za napetost zapisana za približek majhnih deformacij. Deformacija je vsota treh prispevkov. Sestavljajo jo termična deformacija, ki je posledica nehomogenega temperaturnega profila, viskoplastična deformacija, ki je posledica nepovratne deformacije zaradi velikih napetosti v drogu, ter elastična deformacija.

Prostorska diskretizacija enačb modela je izvedena z lokalno kolokacijo z radialnimi baznimi funkcijami, časovna diskretizacija pa z implicitno Eulerjevo metodo. Metoda, ki jo uporabimo za prostorsko diskretizacijo, ustvari aproksimacijo rešitve na lokaliziranih poddomenah z radialnimi baznimi funkcijami in monomi. Iz dobljene aproksimacije lahko izračunamo diskretizacijske koeficiente za vse diferencialne operatorje, ki so prostni v enačbah modela. Ti diskretizacijski koeficienti so uporabljeni v razvitem ogrodju, ki omogoča lažjo sklopitev enačb večfizikalnih modelov in njihovo enostavno časovno diskretizacijo.

Učinkovistost razvite metode je bila preverjena na več različnih testnih

primerih. Natančnost diskretizacijske metode je bila ocenjena z primejavo numeričnih in analitičnih rešitev stacionarnih problemov termomehanike. Posebej zanimivo je obnašanje natančnosti ob spreminjanju oblikovnega parametra, ki določa prostorsko skalo radialnih baznih funkcij. Poleg tega je bil proučen vpliv oblikovnega parametra na pogojenostno število interpolacijskih matrik. Pogojenostno število se je izkazalo za primeren nadomestek oblikovnega prametera kot prosti parameter metode.

Implementacija postopka reševanja je bila preverjena na problemu sklopljenje termoelastičnosti, ki sklaplja transport toplote z elastičnimi valovi. Dobljeni rezultati so bili primerjani z rezultati metode končnih elementov. Rešitvi sta se ujemali za vse obravnavane primere. Ob primerjavi z rešitvijo dobljeno z brezmrežno lokalno metodo Petrov-Galerkin, so se rezultati dobljeni z lokalno kolokacijsko metodo izkazali za bistveno boljše.

Učinkovitost postopka reševanja sistema nelinearnih enaćb dobljenih iz viskoplastičnega mehanskega modela je bila preverjena na kvazi ničdimenzionalnem problemu. Ujemaje rezultatov z analitično rešitvijo je bilo popolno. Rešitev istih enačb na geometrijsko bolj zapletenem primeru je bila primerjana z reštvijo s končnimi elementi. Doblejni rešitvi ta bili praktično enaki, je pa postopek izbire testnega primera izpostavil nekaj pomankljivosti izbranega programa za reševanje s končnimi elementi.

Nazadnje je bila razvita metoda uporabljena za reševanje termomehanskega problema DC ulivanja aluminijevih zlitin. Termomehanski model se za pridobitev nekaterih vhodnih fizikalnih polj zanaša na povezan model prenosa toplote in gibalne količine. Potrebna vhodna fizikalna polja so temperatura, tlak, delež tekoče faze in elektromagnetna sila. Termomehanski model rešuje enačbe na mehansko koherentnem delu kašastega območja, pod položajem izoterme koherenčne temperature. Na območju stika med drogom in kokilo model iterativno določi ustrezne robne pogoje. Ko rešitev mehanskega modela doseže stacionarno stanje, se izračunajo še kriteriji vročega trganja ter profil poroznosti.

Preiskan je vpliv parametrov ulivanja na občutljivost za vroče trganje in poroznost. Model uspešno napove odvisnost v obliki lambda krivulje, ki je tipična za vpliv koncetracije dodanega elementa.

Metoda za prostorsko diskretizacijo se izkaže za sposobno modeliranja

termomehanskih procesov povezanih z DC ulivanjem aluminiujevih zlitin. Rešitve, pridobljene z opisano metodo, so enako učinkovite na neurejenih mrežah kot tudi na urejenih. Preiskave vpliva izbire augmentacijskih polinomov na obnašanje metode kažejo, da je uporaba augmentacije z linearnim polinomom nujna za izboljšanje zanesljivosti metode.

Izdelani model termomehanike med DC ulivanjem, ki sklaplja tok tekočine, vpliv elektromagnetnega polja in prenosa toplote z viskoplastičnim mehanskim modelom, lahko opiše vpliv procesnih parameterov na tvorbo mehanskih napak med DC ulivanjem.

Ključne besede brezmrežne metode, termomehanika, viskoplastičnost, radialne bazne funkcije, lokalna kolokacijska metoda, parameter oblike, DC ulivanje, vroće trganje, poroznost, aluminiujeve zlitine, elektromagnetno ulivanje

Contents

List of Figures

List of Tables

Glossaries

Acronyms

DC	direct chill 6
FDM	finite difference method 5
FEM	finite element method 6
HCS	hot-cracking susceptibility 29
HMTM	heat and momentum transfer model 115
LB	Lahaie-Bouchard 27
LRBFCM	local radial basis function collocation method 41
MLPG	meshless local Petrov-Galerkin method 89
MQ	multiquadric 38
PDE	partial differential equation 4
RBF	radial basis function 4
RPIM	radial point interpolation method 5
SKK	Suyitno-Kool-Katgerman 29

List of symbols

α	coefficient of thermal expansion 15
$\underline{\quad}$	$\underline{y}$ is an array containing discretized values of field y 39
β	thermal coupling coefficient 14

C	fourth-order tensor of elastic moduli 13
d_{as}	dendrite arm spacing 30
$\delta_{\xi\chi}$	Kronecker delta 14
d_g	grain size 28
$\dot{}$	derivative with respect to time: $\dot{T} = \partial T/\partial t$ 15
:	Frobenius inner product. $\boldsymbol{A} : \boldsymbol{B} = \sum_{\xi\chi} A_{\xi\chi} B_{\chi\xi}$ 22
E	Young's modulus 14
$\boldsymbol{\varepsilon}$	strain tensor 10
ϵ	multiquadric shape parameter 38
$\boldsymbol{e}_\kappa$	κ-th vector of orthogonal basis 10
f_l	volume fraction of liquid 30
f_s	volume fraction of solid 30
f_v	volume fraction of voids 30
$f(\sigma)$	yield function 19
G	shear modulus 14
$\mathcal{H}$	plastic history 22
h	node spacing 34
e	L_2 error of the numerical solution 58
λ	Lamé parameter λ 14
${}_lN$	Number of points in the local subdomain l 37
n	power in Norton-Hoff's law 25
$\boldsymbol{n}$	unit normal 11
ν	Poisson's ratio 14
${}_l\Omega$	local subdomain belonging to the point l 36

Q	activation energy 25
$\boldsymbol{r}$	position vector 9
R	general gas constant 25
σ_0	critical stress in Norton-Hoff's law 25
σ_E	elastic limit stress 17
σ_e	effective stress 25
σ_{LB}	critical stress according to LB hot tearing model 29
σ_{SKK}	critical stress according to SKK hot tearing model 31
$\boldsymbol{\sigma}$	stress tensor 11
σ_u	ultimate tensile stress 17
σ_Y	yield stress 17
${}_l s(k)$	mapping returning the index of k-th node in the l-th subdomain 37
$\underline{d}$	solution update calculated by the nonlinear solver 44
$\boldsymbol{t}$	surface traction 11
$\boldsymbol{\tau}$	deviatoric stress tensor 25
T	temperature 14
T_{coh}	coherency temperature 112
T_s	solidus temperature 112
tr	trace of a tensor: $\mathrm{tr}(\boldsymbol{\varepsilon}) = \sum_{\kappa=1}^{3} \varepsilon_{\kappa\kappa}$ 14
T_{ref}	reference temperature 14
$\boldsymbol{u}$	displacement vector 9
$\hat{\boldsymbol{u}}(\boldsymbol{r})$	deformation vector field which is the exact solution of a mechanical problem 59
U	stress energy function 22

w	strain energy function 14

Chapter 1

Introduction

1.1 Motivation

The fast progress of computer capability illustrated by Moore's law has enabled great advancements in numerical modeling in engineering and science. This advancement was accompanied by development of classical numerical methods: the finite element method, finite difference method and finite volume method. These methods have earned the reputation of reliable tools in computer-aided engineering and science.

However, the need for numerical models and the quest for knowledge have jointly driven the development of new numerical methods and increasingly more sophisticated physical models. The new, sophisticated models, have often hit the limitations of the classical methods. The classical methods are difficult to use when they are applied to problems which require changing of the underlying mesh, be it because the movement of the mesh points is required by the physical model or because some form of adaptive mesh refinement needs to be implemented. The classical methods, especially the finite difference method, can also have problems when dealing with complex geometries. The formulations of the classical methods themselves can significantly change when considering higher-dimensional problems. This is especially evident for the finite element method, since each new spatial dimension introduces a set of new geometrical objects, which need to be constructed and kept track of.

All the limitations stated above are caused by the requirement of the

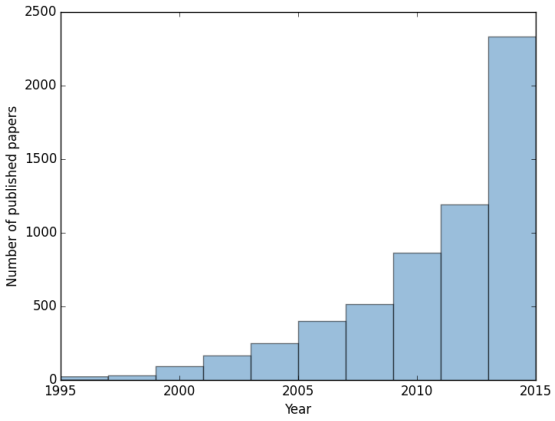

FIGURE 1.1: Number of published papers per year containing keywords "meshless" or "meshfree" as returned by Google Scholar search on 30th November 2016.

classical methods to be formulated not only on a set of points but on a set of points with an associated structure, which could limit the positioning of points or could require additional connectivity information (e.g. polygonization) to be constructed. The removal of the requirement for this kind of associated structure or even just its simplification would increase the flexibility of the method and possibly allow for more efficient solution of the problems or allow description of problems unapproachable by the classical methods.

The methods which aim to reduce the compexity of the associated structure or even remove the need for mesh altogether are called meshless (or meshfree) methods. As illustrated by the Figure 1.1 this class of methods is receiving increasingly more attention from the modeling community. In this work, we contribute to this corpus by applying a meshless method to modeling of mechanical phenomena during DC casting of aluminium billets.

1.2 Overview of meshless methods

The name meshless methods is used to describe many different methods. The most important distinction between the methods is the approach which is used to discretize the governing equations. The largest class of methods applies Galerkin approach of rewriting the governing equation in weak form

and expressing the integrals in terms of the selected approximation function. The other class, which also includes the method used in this work, consists of methods which use collocation. The governing equation is discretized by directly evaluating the derivatives of the approximation function in discretization points.

Another way to classify the methods is by the way they construct the approximation function (Wendland, 2004). Regardless of the method used, the aim of the approximation is to construct the Lagrange functions $\Lambda_i(\boldsymbol{r})$, which are such that given a set of points $\{\boldsymbol{r}_l; l = 1 \dots n\}$ a function $\phi(\boldsymbol{r})$ is sufficiently well approximated in point $\boldsymbol{r}$ near the set $\{\boldsymbol{r}_l; l = 1 \dots n\}$ by approximation $s(\boldsymbol{r})$

$$s(\boldsymbol{r}) = \sum_{i=1}^{n} \phi(\boldsymbol{r_i})\Lambda_i(\boldsymbol{r}). \tag{1.1}$$

Roughly, we can distinct three kinds of approximation approaches, depending on the way the Lagrange function is determined. The reproducing kernel approach assumes an expression for the Lagrange function, while the moving least squares and interpolation approaches use Lagrange function which is calculated by using least squares approximation and interpolation conditions, respectively. Described approximation approaches also differ in the accuracy of constructed approximation functions. For a given number of local points, the interpolation, which is used in this work, is usually the most accurate.

The last distinction between the methods can be made with respect to the type of basis functions which are used to construct the approximation. Mostly, the methods use low order polynomials, especially when using the least-squares to construct the approximation. The minority of methods uses other basis functions, which try to avoid the setbacks of polynomials. The method used in this dissertation is of latter kind and uses radial basis functions to construct the approximation function.

The method which is used in this dissertation belongs to collocation meshless methods which use interpolation with radial basis functions to construct local approximation function. This kind of methods are relatively recent additions to the family of meshless methods, being developed only since the start of the new millennium, although, as we see in the next section, the ideas employed are significantly older.

1.2.1 Historical development of local collocation meshless methods

The first step in the development of the meshless methods was the idea presented by Jensen in 1972 (Jensen, 1972). He proposed a system for generation of finite differences on irregular grids using interpolation with polynomials on local stencils consisting of a small number of nearest neighbors. His method was pestered by poorly conditioned interpolation matrices and a stencil modification had to be used when a poorly conditioned stencil was encountered. This problem was remedied in the paper by Liszka and Orkisz in 1979 (Liszka and Orkisz, 1979). Their solution was to use a weighted least-squares approximation by second order polynomial constructed from the values in the stencil. They successfully applied the developed method to a selection of problems in solid mechanics. The use of the least squares is not the only way to stabilize the interpolation problem. The replacement of polynomials with positive definite radial basis functions (RBFs) has the same effect (Buhmann, 2003).

The superior properties of radial basis functions were demonstrated by extensive test of different scattered data approximation schemes in the work of Franke (Franke, 1982). He performed the tests of 29 different scattered data approximation techniques and found the interpolation with radial basis functions to be superior to other approaches.

The seminal work by Kansa (Kansa, 1990a; Kansa, 1990b) was the first application of RBFs to numerical solving of partial differential equations (PDEs). In his two papers he first demonstrated capabilities of RBFs to accurately calculate the derivatives. This allowed him to use the method to solve parabolic, hyperbolic and elliptic equations in two dimensional setting. The detailed theory of the convergence of the method was developed later on by Franke (Franke and Schaback, 1998). Since the RBF interpolant used by Kansa was constructed using all the points in the computational domain, the resulting interpolation matrix was dense and ill-conditioned. These problems overwhelmed very good convergence properties of the method, and the approach failed to gain widespread adoption. However, the idea of using RBFs for construction of approximations in numerical methods lived on.

The RBF interpolation reemerged a few years later in work done on the boundary elements method, although in a different setting. The particular solution of the governing equation was determined by integrating the RBF interpolant of the source term. Initially, conical functions were used (Partridge et al., 1992), but were soon replaced by RBFs because of their superior interpolation properties (Golberg and Chen, 1994; Golberg, 1995). The idea of integrating the interpolants instead of differentiating them gained wide popularity and is still developed today (Yao et al., 2015; Zhang et al., 2016).

The next application, for which good interpolation properties of RBFs were demonstrated, was the radial point interpolation method (RPIM) (Gu and Liu, 2001). It used RBFs to construct local interpolation which was used to discretize weak form equations for solid mechanics.

Soon after that, a group of papers appeared, which locally constructed RBF interpolant and used it so solve strong formulation equations (Tolstykh and Shirobokov, 2003; Lee et al., 2003; Liu et al., 2002). Interestingly enough, two of those three papers dealt with solid mechanics problems. From then on, the approach gained quite wide adoption and was used to model wide spectrum of problems ranging from thermal transport (Šarler and Vertnik, 2006), fluid flow (Divo and Kassab, 2007), geophysics (Flyer et al., 2012), reaction-diffusion problems on surfaces (Shankar et al., 2015) to problems in solid state physics (Kosec and Trobec, 2015).

The method used in these papers calculates the derivatives by analytic derivation of the interpolant. The other option is the approach presented in (Liu et al., 2006), where the finite difference method (FDM) is used to construct the derivatives. The RBF interpolant is used only to interpolate the values from the disordered mesh points onto a finite difference stencil, which is then used to calculate the derivatives by the finite difference method. This approach has also been successfully applied to many problems in engineering (Gerace et al., 2013), especially where stable calculation of advection is necessary (Harris et al., 2015).

Our choice of the local RBF collocation method to perform the work done in this dissertation was greatly influenced by the successful application of the approach to several industrial problems related to solidification of metals (Vertnik, 2010; Kosec et al., 2011; Mramor, 2015) and large plastic

deformation during thermomechanical processing of steel (Hanoglu, 2015).

1.3 Overview of thermomechanics DC casting models

The direct chill (DC) casting of aluminium is well established procedure and a lot of effort has been spent designing models which describe it. The models of solid mechanics, which already included elasto-plastic constitutive models (Weiner and Boley, 1963), were the first addition to the models of solidification. The models were designed before wide availability of computational resources and thus provided analytic expressions connecting the process parameters to the stress state of the cast piece.

The first model of thermomechanics during direct chill casting was formulated for casting of aluminium slabs (Tien and Koump, 1969). They considered a beam-shaped section of the solidifying slab and determined the dependence of stresses and displacements of the surface on thickness and cooling rate.

The switch from analytic models to numerical models was essential to achieve widespread use of the models. The first such model was presented in (Williams et al., 1979). They modeled the process of continuous casting of steel by considering heat transfer and elasto-viscoplastic model of solid mechanics. Their model used finite element method (FEM) to discretize the governing equations. Such model already included most of the important physics and its usability is reflected in additional improvements in subsequent years (Fjaer and Mo, 1990; Zabaras et al., 1990).

Another important addition to the models was the inclusion of the effects of fluid flow. This was first included in the work (Li and Ruan, 1995), which considered casting of a cylindrical billet and was also stated using FEM. This model indicated the development of the field in the subsequent years. The developed models were getting more complicated by including two-phase models of the mushy zone (Farup and Mo, 2000) and increasingly complicated rheological models (M'Hamdi et al., 2006) to improve the description of the mushy zone. Such models provide results in terms of the stress and the strain fields, porosity and the hot-tearing susceptibility.

In recent years the great insights have been achieved also by large-scale microscopic models (Phillion et al., 2009). Their resolution at the scale of grains includes description of the inter-granular liquid channels (Vernède et al., 2009; Sistaninia et al., 2013b). Such models have been applied also to the problem of DC casting (Sistaninia et al., 2013a) to accurately predict the location of crack initiation and growth direction.

1.4 Goals

The research group of prof. Šarler pioneered the use of meshless method for modeling multiphase processes in material processing. The phenomena that were successfully modeled were very diverse. The first was the modeling of solid-solid phase changes in homogenization of aluminium alloys (Kovačević and Šarler, 2005) which was followed by thermal models of DC casting of aluminium (Vertnik et al., 2006).

Considerable amount of work has been done on modeling continuous casting of steel. A model considering solidification, fluid flow, thermal transport, species transport and turbulence was developed for two-dimensional and three-dimensional descriptions of the process (Vertnik and Šarler, 2009; Vertnik and Šarler, 2016). Model of electromagnetic braking during the continuous casting process were added in (Mramor, 2015). Meshless methods were also used in development of traveling slice models of continuous casting of steel (Vušanović et al., 2011). The model considered thermal transport, solidification and grain growth. Similar concept of traveling slice was used to model hot-rolling of steel (Hanoglu et al., 2011). The model was stated in Lagrangian formulation to describe heat transfer and deformation of the material.

Although the DC casting of aluminium was the first process which was modeled by a meshless method, no additional progress was done in this until recently. The model was upgraded by addition of fluid flow and electromagnetic stirring (Košnik et al., 2014; Hatić et al., 2016). Development of a meshless model which would complement this work by providing results considering thermomechanical aspects of the process is the main goal of this dissertation.

Te model is also expected to provide a way to predict occurrence of mechanical casting defects, the main goal being the prediction of hot tearing. We also aim to predict the occurence of porosity and the shape of the billet surface.

Considering a lack of literature on the application of the local radial basis function to problems in viscoplasticity and thermomechanics the goal is also to devise numerical methods which enable a stable and robust solution of the considered model and provide further insight in the performance of the method.

Chapter 2

Physical background

In this chapter we expose the physical background of the approach used to assemble the model of DC casting by describing the framework of solid mechanics, following the approach of (Fung and Tong, 2008) and the viscoplasticity theory, specifically the approach of viscoplastic potentials as exposed in (Simo and Hughes, 1998) and (Lubarda, 2002).

2.1 Mechanics

2.1.1 Description of strain

The description of the configuration of the deformed body is essential for formulation of solid mechanics. It is achieved by two quantities, the displacement and strain. We start by considering the situation illustrated in Figure 2.1. The body is deformed from configuration Ω to the configuration denoted Ω'. The deformation of the body moves the material which was at position $\boldsymbol{r}$ to the position $\boldsymbol{R}(\boldsymbol{r})$. The difference between the two positions is called the displacement $\boldsymbol{u}$ and is defined by

$$\boldsymbol{u}(\boldsymbol{r}) = \boldsymbol{R}(\boldsymbol{r}) - \boldsymbol{r}. \tag{2.1}$$

We assume that the displacement is continuous, which means that no cracks or holes are introduced into the body by the deformation. Also, to simplify the formulation, we require the displacements to be twice continuously differentiable.

The stress that develop in the body because of the deformation are not determined directly by the displacement. A rigid body motion does not induce any stress within the body although, it results in nonzero displacement. The source of stress is the stretching and torsion that are imposed on the body by the deformation.

To determine the quantity of interest, we study the length of vector $\mathrm{d}\boldsymbol{r}$, which connects two nearby material points. The deformation maps this vector to the vector $\mathrm{d}\boldsymbol{R}$. In coordinate system with basis vectors $\{\boldsymbol{e}_\kappa,\ \kappa = 1, 2, 3\}$ the vector $\mathrm{d}\boldsymbol{r}$ is

$$\mathrm{d}\boldsymbol{r} = \sum_{\kappa=1}^{3} \mathrm{d}x_\kappa \boldsymbol{e}_\kappa. \tag{2.2}$$

Inverting the equation (2.1), the change of length of the vector $\mathrm{d}\boldsymbol{r}$ is given by

$$|\mathrm{d}\boldsymbol{R}|^2 - |\mathrm{d}\boldsymbol{r}|^2 = \sum_{\xi,\kappa=1}^{3} \left[(\boldsymbol{I} + \nabla\boldsymbol{u})^T (\boldsymbol{I} + \nabla\boldsymbol{u}) - \boldsymbol{I} \right]_{\xi\chi} \mathrm{d}x_\xi \mathrm{d}x_\chi. \tag{2.3}$$

The matrix in front of the factor $\mathrm{d}x_\xi \mathrm{d}x_\chi$ is proportional to the strain tensor $\boldsymbol{\varepsilon}$. Its components are given as

$$\varepsilon_{\xi\chi} = \frac{1}{2} \left(\frac{\partial u_\xi}{\partial x_\chi} + \frac{\partial u_\chi}{\partial x_\xi} + \frac{\partial u_\xi}{\partial x_\chi} \frac{\partial u_\chi}{\partial x_\xi} \right). \tag{2.4}$$

When the components of the displacement vector gradient are small, the nonlinear term can be neglected. The linearized strain is then given by

$$\varepsilon_{\xi\chi} = \frac{1}{2} \left(\frac{\partial u_\xi}{\partial x_\chi} + \frac{\partial u_\chi}{\partial x_\xi} \right). \tag{2.5}$$

This definition of strain will be used in the rest of the dissertation.

The aim of this dissertation is modeling viscoplastic deformations, which develop during the proces of DC casting. Usually, viscoplasticity is associated with large deformation of the material. In the case of DC casting we know from the observation of the process itself, that the strains are small, on the order of 0.01. This gives us confidence in the decision to use the small strain approximation.

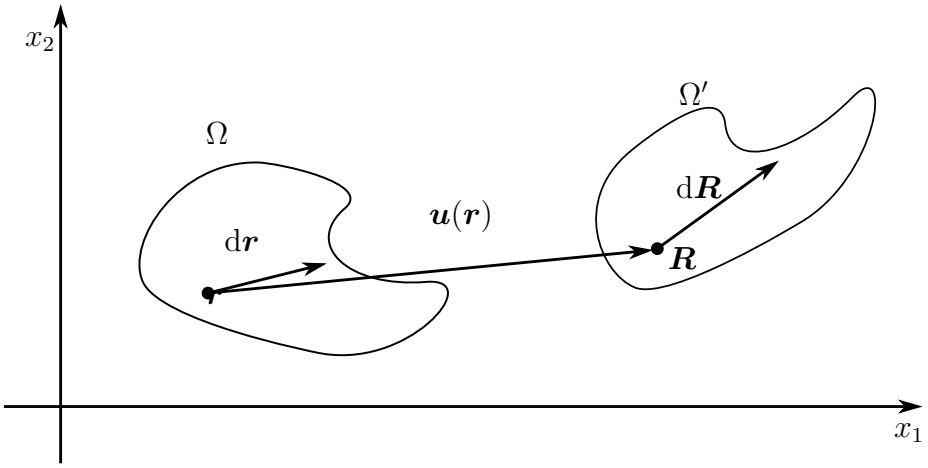

FIGURE 2.1: Definition of displacement.

2.1.2 Description of stress and stress equilibrium

To formulate the definition of stress tensor, we need to consider a closed surface Γ inside a body, illustrated in Figure 2.2. If there are stresses present in the body, then we can assume that a force $\mathrm{d}\boldsymbol{F}$ is acting on each small part $\mathrm{d}S$ of the surface. The ratio of these two quantities is called traction $\boldsymbol{t}$. The linear mapping, which maps the normal of the surface element $\boldsymbol{n}$ to the traction prescribed on the surface element is the stress tensor $\boldsymbol{\sigma}$. It can be implicitly defined as

$$t_\xi = \sum_{\chi=1}^{3} \sigma_{\xi\chi} n_\chi. \tag{2.6}$$

The stress in the body is tightly connected with the deformation of the body, which is described by strain.

Using the same setting, we can also derive the stress equilibrium condition. Let us first allow for an additional external body force to be acting on the considered body. The distribution of the force can be described with $\boldsymbol{f}(\boldsymbol{r})$. The force equilibrium for the body Ω with surface Γ is given by

$$\oint_\Gamma \boldsymbol{t}\mathrm{d}\Gamma + \int_\Omega \boldsymbol{f}\mathrm{d}V = 0. \tag{2.7}$$

The definition (2.6) is used to express the equilibrium condition in terms of stress tensor. Using the divergence theorem, we arrive at

$$\int_\Omega (\nabla \cdot \boldsymbol{\sigma} + \boldsymbol{f})\,\mathrm{d}V = 0. \tag{2.8}$$

By reducing the volume of the interior of the surface to such extent that the integration term can be assumed constant, we see that the equilibrium condition is

$$\nabla \cdot \boldsymbol{\sigma} + \boldsymbol{f} = 0. \tag{2.9}$$

If the body is not in equilibrium, it starts accelerating as specified by the following equation of motion

$$\nabla \cdot \boldsymbol{\sigma} + \boldsymbol{f} = \rho \ddot{\boldsymbol{u}}, \tag{2.10}$$

where ρ is the mass density.

Besides the equilibrium of forces, we also need to consider the equilibrium of torques. The torque of the tractions acting on surface of the body Γ is given as

$$M_{\xi\chi} = \oint_{\Gamma} \left(t_\xi x_\chi - t_\chi x_\xi\right) \mathrm{d}\Gamma = \sum_{\zeta=1}^{3} \oint_{\Gamma} \left(\sigma_{\xi\zeta} x_\chi - \sigma_{\chi\zeta} x_\xi\right) n_\zeta \mathrm{d}\Gamma. \tag{2.11}$$

The same torque can be also calculated by the integration of the body force induced by stress $\boldsymbol{\sigma}$ over the volume Ω of the body.

$$M_{\xi\chi} = \int_{\Omega} \left(\nabla \cdot \boldsymbol{\sigma}_\xi x_\chi - \nabla \cdot \boldsymbol{\sigma}_\chi x_\xi\right) \mathrm{d}V = \sum_{\zeta=1}^{3} \int_{\Omega} \left(\frac{\partial \sigma_{\xi\zeta}}{\partial x_\zeta} x_\chi - \frac{\partial \sigma_{\chi\zeta}}{\partial x_\zeta} x_\xi\right) \mathrm{d}V. \tag{2.12}$$

This expression can be rewritten in terms of the surface integral in equation (2.11) and an additional term

$$\int_{\Omega} \sum_{\zeta=1}^{3} \left(\sigma_{\xi\zeta} \frac{\partial x_\chi}{\partial x_\zeta} - \sigma_{\chi\zeta} \frac{\partial x_\xi}{\partial x_\zeta}\right) \mathrm{d}V, \tag{2.13}$$

which should be equal to zero, since the equations (2.11) and (2.12) define the same physical quantity. This is only possible if $\sigma_{\chi\xi} = \sigma_{\xi\chi}$, which means that the stress tensor has to be symmetric.

The stress tensor is real-valued and symmetric, which means that its eigenvalues are real and that the corresponding set of eigenvectors is orthogonal. The eigenvalues are called the principal stresses and the directions defined by the eigenvectors are called principal directions. In each principle direction the material experiences pure tension/compression with its amplitude given by the corresponding principal stress.

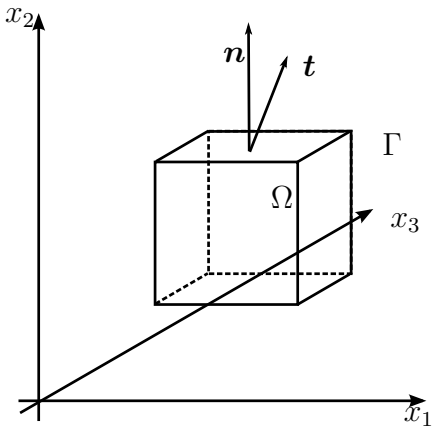

FIGURE 2.2: Illustration to definition of stress.

In the derivations above we have omitted an important detail. In general, all the integrations in the above expressions should be performed on control volumes in the deformed body. However, in numerical models, the equations are usually stated for the undeformed configuration, although the stress equilibrium should be achieved in the deformed configuration. One can imagine that significant rotation of the material caused by the deformation could cause the directions of surface normals to change and thus also changing the direction of the tractions resulting in wrong solution of the equilibrium equation. Our approximation is thus only valid if the rotation caused by the deformation is small. This can be controlled for by factoring the deformation gradient as

$$\nabla \boldsymbol{R} = \boldsymbol{Q}\boldsymbol{S}, \tag{2.14}$$

which is the usual QR decomposition where $\boldsymbol{Q}$ is orthogonal and the matrix $\boldsymbol{S}$ is upper triangular. This decomposition splits the deformation in two parts. A vector $\mathrm{d}\boldsymbol{x}$ in the original configuration is first deformed by the matrix $\boldsymbol{S}$ and then rotated by $\boldsymbol{Q}$ to become $\mathrm{d}\boldsymbol{X}$ in the deformed configuration. We can neglect the fact that the equilibrium equations are stated for the undeformed configuration instead for the deformed one, as long as the rotation given by $\boldsymbol{Q}$ is small (Fung and Tong, 2008).

2.1.3 Linear theory of thermoelasticity

To be able to write the equilibrium condition (2.10) in terms of deformation vector, we need to assume a constitutive law connecting the stress and strain tensors. The most general linear law of this form is specified by a fourth order elastic tensor C by $\boldsymbol{\sigma} = \boldsymbol{\varepsilon}$. In case of an isotropic body, only two constants are enough to describe the tensor C. This special case is known as the Hooke's law and is given by

$$\sigma_{\xi\chi} = \lambda \operatorname{tr}(\boldsymbol{\varepsilon})\delta_{\xi\chi} + 2G\varepsilon_{\xi\chi}. \tag{2.15}$$

The λ stands for Lamé parameter and G for the shear modulus. The $\delta_{\xi\chi}$ symbol stands for Kronecker delta and tr is the trace of the tensor. There are many different parametrizations of the Hooke's law. The one used in formula (2.15) is usually used in physics. In engineering, use of Young's modulus E and Poisson's ratio ν is more common. The connections between them are

$$\lambda = \frac{\nu E}{(1-2\nu)(1+\nu)} \tag{2.16}$$

$$G = \frac{E}{2(1+\nu)}. \tag{2.17}$$

For uniaxial loading of the material, the Young's modulus directly connects the stress $\sigma_{\parallel}$ and the strain $\varepsilon_{\parallel}$ by $\sigma_{\parallel} = E\varepsilon_{\parallel}$. In the same setting, the Poisson's ratio connects the strain in the axial direction with the strain in the orthogonal direction $\varepsilon_{\perp} = \nu\varepsilon_{\parallel}$.

The derivation of the coupling with temperature field T requires a short detour in thermodynamics. We introduce the strain energy function w defined by

$$\mathrm{d}w = \sum_{\xi,\chi=1}^{3} \sigma_{\xi\chi}\mathrm{d}\varepsilon_{\xi\chi}. \tag{2.18}$$

It can be shown that such a function describes the internal energy of an isentropic process or the Helmholtz free energy of isothermal process (Fung and Tong, 2008). In case of an isotropic solid, this function can be written as

$$w = \frac{\lambda}{2}(\operatorname{tr}(\varepsilon))^2 + G\sum_{\xi,\chi=1}^{3} \varepsilon_{\xi\chi}\varepsilon_{\xi\chi}. \tag{2.19}$$

To describe the thermoelastic coupling we need to introduce additional terms in the strain energy function. The lowest order contribution is of the

first order in both, strain and temperature. New strain energy function for isotropic solid has therefore the form

$$w = \frac{\lambda}{2}(\,\mathrm{tr}(\varepsilon))^2 + G\sum_{\xi,\chi=1}^{3}\varepsilon_{\xi\chi}\varepsilon_{\xi\chi} - \beta(T - T_{ref})\,\mathrm{tr}(\varepsilon). \tag{2.20}$$

In this expression β is the coefficient describing thermal expansion and T_{ref} is the reference temperature, at which we assume the thermal stresses to be zero. Using the definition of the strain energy function (2.18), the strain tensor definition (2.5), and the equilibrium equation (2.10) we can obtain the equilibrium equation in terms of the displacement

$$G\nabla^2\boldsymbol{u} + (G+\lambda)\nabla\nabla\cdot\boldsymbol{u} = \nabla\Big(\beta\,(T - T_{ref})\,\Big) - \boldsymbol{f} \tag{2.21}$$

and, for non-equilibrium conditions,

$$\rho\ddot{\boldsymbol{u}} = G\nabla^2\boldsymbol{u} + (G+\lambda)\nabla\nabla\cdot\boldsymbol{u} - \nabla\Big(\beta\,(T - T_{ref})\,\Big) + \boldsymbol{f}. \tag{2.22}$$

The coefficient β is given by $\beta = \alpha E/(1-2\nu)$, where α is the coefficient of linear expansion defined in the relation

$$\varepsilon_{\xi\chi} = \delta_{\xi\chi}\alpha(T - T_{ref}). \tag{2.23}$$

By using this approach, we manage to obtain the coupling in one direction only, namely for a given temperature field, we are able to calculate the impact on stresses. To achieve thermodynamic consistency, we should also account for the inverse coupling. The derivation of the coupling comes from the consideration of the rate of entropy production (Fung and Tong, 2008). In order to simplify the equations we use thermodynamic quantities given per unit mass, e.g. $F = \int \rho f \mathrm{d}V$. The entropy production rate is given by

$$\rho\dot{s} = \rho\frac{\partial s}{\partial\varepsilon_{\xi\chi}}\dot{\varepsilon}_{\xi\chi} + \rho\frac{\partial s}{\partial T}\dot{T}. \tag{2.24}$$

The dot ($\dot{}$) over a physical quantity stands for partial derivative with respect to time $\dot{T} = \partial T/\partial t$. From the thermodynamics we know the connection between the entropy production rate and the heat flux $\boldsymbol{j}$

$$\rho\dot{s} = -\frac{1}{T}\nabla\cdot\boldsymbol{j} \tag{2.25}$$

and the definition of the heat capacity at constant volume

$$c_v = -T\frac{\partial^2 F}{\partial T^2}. \tag{2.26}$$

Our aim is to rewrite the equation (2.24) in terms of free energy. The free energy of an isotropic elastic material is given by

$$\rho f = w - \rho T s, \tag{2.27}$$

where w is the strain energy function. From the free energy definition it is clear that we have $-s = \partial f/\partial T$. The equation (2.24) can now be written in terms of free energy and heat flux

$$-\frac{1}{T}\vec{\nabla}\cdot\boldsymbol{j} = -\rho\sum_{\xi,\chi=1}^{3}\frac{\partial f}{\partial\varepsilon_{\xi\chi}\partial T}\dot{\varepsilon}_{\xi\chi} - \rho\frac{\partial^2 f}{\partial^2 T}\dot{T}. \tag{2.28}$$

The definitions of heat capacity and free energy can be used to replace the partial derivatives of the free energy. By employing the definition of the heat flux from Fourier's law $\boldsymbol{j} = -k\vec{\nabla}T$ we get the coupling equation that we were looking for

$$\sum_{\xi=1}^{3}\frac{\partial}{\partial x_\xi}\left(k\frac{\partial T}{\partial x_\xi}\right) = \rho c_v\dot{T} + T\beta\,\mathrm{tr}(\dot{\varepsilon}). \tag{2.29}$$

One can imagine that the physical problems governed by the equations listed above are quite difficult to solve. In order to obtain results which are relevant in engineering, we have to introduce some simplifications. The equations that we have written deal with transient problems, so the straightforward simplification is to limit ourselves to quasi-static problems, where all the fields are assumed to be stationary.

The fact that the adiabatic expansion of the gas is accompanied by a drop in its temperature is known as Joule-Kelvin phenomenon (Žumer and Kuščer, 2006). The equation describing the same phenomenon for solids can be obtained from equation (2.29), by forbidding the heat conduction ($\vec{j} = 0$). This gives us the equation connecting the rate of change of temperature with the strain rate

$$\frac{\partial T}{\partial t} = -\frac{T\beta}{\rho C_v}\,\mathrm{tr}(\dot{\varepsilon}). \tag{2.30}$$

The coefficient in front of the strain rate has in case of aluminium value $\approx$ 1K. To estimate the strain rate, we assume that all the boundary conditions

and body forces are stationary. The only contribution to the strain rate is then the thermal expansion given by (2.23). The increase of temperature $\mathrm{d}T$ in time interval $\mathrm{d}t$ is then the sum of the increase due to the thermal conduction $\mathrm{d}T_{con}$ and the increase due to the strain rate $\mathrm{d}T_{\varepsilon}$. The increase of the temperature is then $\mathrm{d}T = (1 + \alpha 1\,\mathrm{K})\mathrm{d}T_{con}$. Since the value of α is approximately $10^{-5}K^{-1}$, the contribution to the temperature increase due to the strain rate is negligible.

2.2 Viscoplasticity

2.2.1 Motivation

The linear constitutive law is a good approximation for material behavior only in narrow, but important, range of loading. The behavior predicted by linear law is appropriate only when the applying load results in small deformations. To describe materials in general load configurations, we need to consider more complicated, nonlinear, material models.

In Figure 2.3 a typical stress-strain curve of an aluminium alloy is shown by the solid line (Hill, 1998). The linear model applies when stresses are below the elastic limit stress, denoted by σ_E. As we increase the strain, we reach the yield stress σ_Y, when the plastic deformation starts to be significant. The yield stress is the stress at which a given amount of plastic deformation occurs, the yield value being dependent on the selected amount of plastic deformation. In literature, usually value of 0.2% is used. As we increase the load further, we reach the ultimate tensile stress σ_u, which is the largest stress the material can support. Further increase in stress is not possible. The strain, however, can be increased further, but the stress decreases when doing so. This is only possible until we reach the fracture point $(\varepsilon_f, \sigma_f)$, when the material fractures.

All this parameters are still not enough to completely describe the behavior of aluminium alloys, particularly at high temperatures. The strain rate, which is used to obtain the curve in the experiments, can change the shape of the curve, as indicated in Figure 2.3. In the experiments the values ranging from 10^{-1} to $10^{-7}\mathrm{s}^{-1}$ can be used (Kassner and Pérez-Prado, 2004).

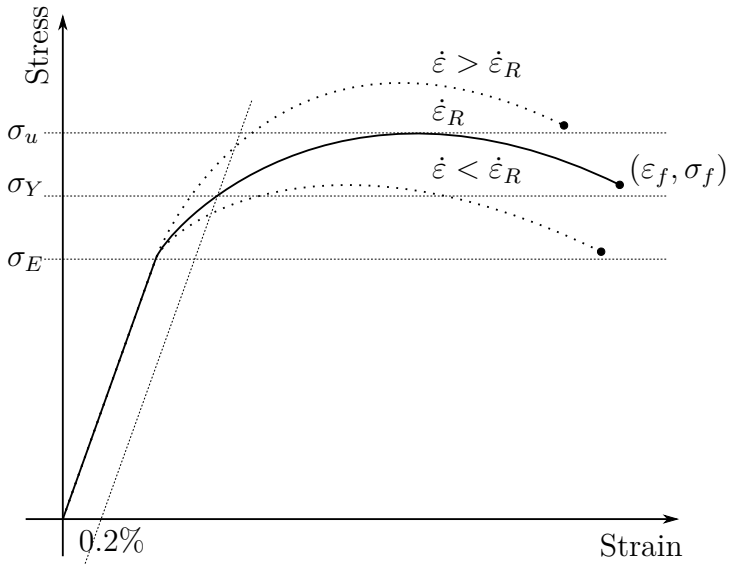

FIGURE 2.3: Typical stress strain curve of an aluminium alloy.

Larger strain rate can increase both, the observed yield stress and the ultimate tensile strength (Chen et al., 2009; Ludwig et al., 2005). In the Figure 2.3 two additional stress-strain curves are plotted with dots for strain rates larger and smaller than the curve obtained by the reference strain rate. When the yield stress depends on the stress rate, the material is said to be viscoplastic (Hill, 1998).

2.2.2 Toy-model of viscoplasticity

More insight in the behavior of a viscoplastic metal can be obtained by considering the one dimensional model shown in Figure 2.4 (Simo and Hughes, 1998). Such toy-models are often used to intuitively understand viscoelasticity (Fung and Tong, 2008). A simple model for viscoplasticity can be constructed by slightly modifying the model for Maxwell viscoelastic material (Fung and Tong, 2008). The Maxwell model, contained in the blue shaded area in Figure 2.4, consists of connection of spring element with elastic constant E and a dashpot with time constant η in series. Plastic behavior is added to the model by connecting a friction element with yield stress σ_Y in parallel to the dashpot.

The total strain of the device is the sum of elastic part ε^e and the plastic

part ε^p. The elastic part is the strain of the spring. The stress on the device can be calculated as

$$\sigma = E\varepsilon^e = E(\varepsilon - \varepsilon^p). \tag{2.31}$$

If the stress σ is smaller than the σ_Y all the stress can be transferred by the friction device with no stress acting on the dashpot. However, when the absolute value of the stress is larger than the yield stress, the dashpot starts to move in such a manner that the extra stress is transferred by it. The extra stress is given by

$$\sigma_{ex} = (|\sigma| - \sigma_Y)\text{sign}(\sigma) \tag{2.32}$$

From the constitutive equation of the dashpot $\sigma = \eta\dot{\varepsilon}^p$ we can obtain the equation for the viscoplastic strain rate

$$\dot{\varepsilon}^p = \frac{1}{\eta}(|\sigma| - \sigma_Y)\text{sign}(\sigma), \tag{2.33}$$

if

$$|\sigma| - \sigma_Y \geq 0. \tag{2.34}$$

The criterion in the equation (2.34) is called the yield criterion. Usually, it is specified by a yield function $f(\sigma)$, which is defined in such a manner that when $f(\sigma) < 0$ the material behaves elastically and when the $f(\sigma) > 0$ plastic deformation occurs. The generalized surface in stress space given by the equation $f(\sigma) = 0$ is called the yield surface. In general, it is usually a generalized prism or a cone in space of principal stresses. In our case, however, it is especially simple, since it is only a pair of points on the stress line at $\sigma = \pm\sigma_Y$. Using the definition of yield function, the viscoplastic strain rate is given by

$$\dot{\varepsilon}^p = \frac{1}{\eta}f(\sigma)\text{sign}(\sigma), \tag{2.35}$$

if $f(\sigma) \geq 0$.

Two physically interesting behaviors can be observed by considering two different ways of loading the system. The first one can be observed if a finite strain ϵ_0 is instantaneously applied on the device. This can be described by a step function in strain

$$\varepsilon = \varepsilon_o H(t). \tag{2.36}$$

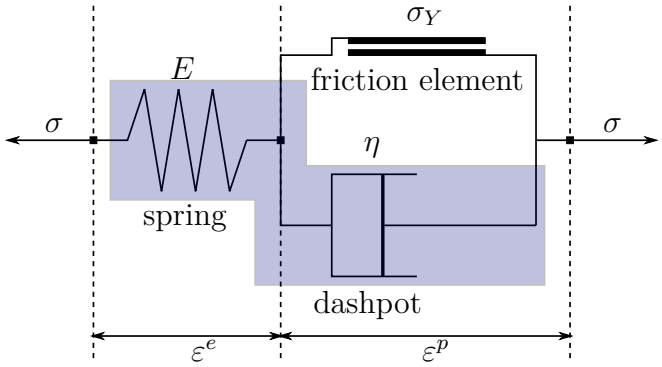

FIGURE 2.4: One dimensional toy-model of viscoplasticity.

Here, $H(t)$ denotes the Heaviside step function. To observe the plastic behavior, the amplitude of the applied strain must be large enough to cause stresses larger than the yield stress, $E\varepsilon_0 > \sigma_Y$.

Taking the time derivative of the constitutive equation for stress (2.31) and combining it with the plastic strain rate equation (2.33) we obtain the following ordinary differential equation for stress

$$\dot{\sigma} = -\frac{E}{\eta}(\sigma - \sigma_Y). \tag{2.37}$$

With initial condition $\sigma(t = 0) = E\varepsilon_0$. This equation describes the exponential decay of the stress towards the yield stress as the stationary state is approached.

The second important phenomenon can be observed if we consider the stationary state when a constant strain rate $\dot{\varepsilon_0}$ is being applied to the system. The constant strain rate will only cause the elastic deformation of the spring until the yield limit is reached $E\varepsilon \leq \sigma_Y$. After that, the plastic strain rate will be nonzero and governed by the equation

$$\dot{\varepsilon}^p = \frac{1}{\eta}(\sigma - \sigma_Y). \tag{2.38}$$

The governing equation for stress can be obtained by time differentiation of the equation (2.31). The stationary state of stress is reached when $\dot{\varepsilon}^p = \dot{\varepsilon}_0$. From the equation (2.38) it follows that the stationary stress σ_∞ is

$$\sigma_\infty = \sigma_Y + \eta\dot{\varepsilon}_0. \tag{2.39}$$

This result demonstrates that the material can sustain stresses larger than the yield stress. The extra stress the material can sustain depends on the rate

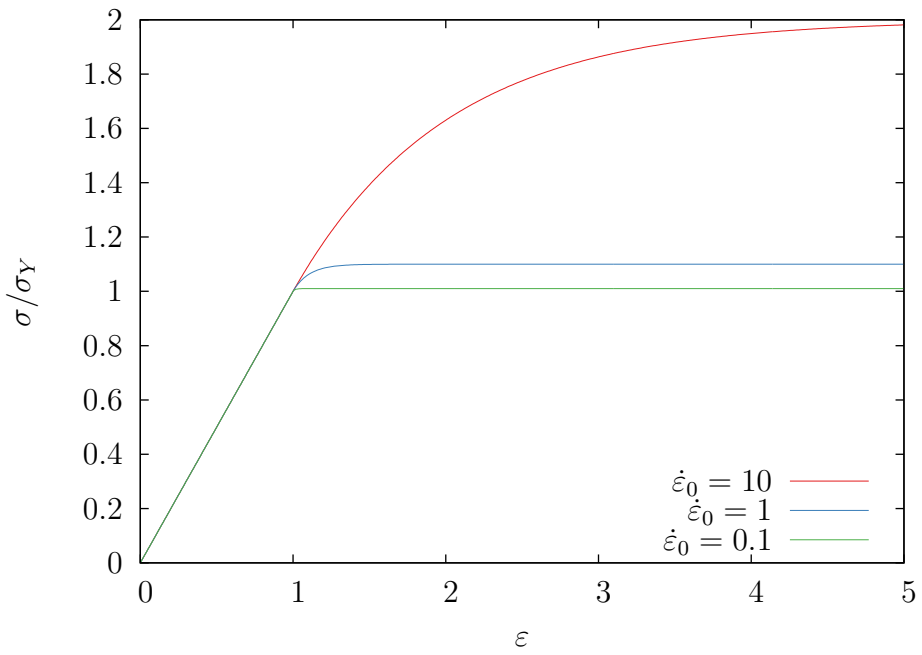

FIGURE 2.5: Stress-strain curves of one dimensional viscoplastic model ($E = 1$, $\eta = 0.1$, $\sigma_Y = 1$).

of deformation. Stress-strain curves for the toy-model subject to constant strain rate are shown in Figure 2.5. We see that the larger the strain rate, the larger is the extra stress that the material can sustain. Such behavior is a feature of the stress-strain curve shown in Figure 2.3, demonstrating that viscoplasticity can be used to describe the observed behavior.

2.2.3 Rate-dependent plasticity via viscoplastic potentials

For many years the approach to the modeling of viscoplasticity was in principle the same as the one illustrated by the toy-model. The plastic region determined by the yield function was used to determine the area where the material behaves elastically. In the plastic regime, the plastic strain rate was determined by a constitutive law similar to the equation (2.33). In recent years, however, a different approach is gaining traction. The yield function and associated viscoplastic strain rate equation is replaced by a viscoplastic potential, which is used to determine the viscoplastic strain rate (Hill and Rice, 1973). Such models are especially well suited for

modeling of heterogeneous materials such as soil (Kelln et al., 2008), concrete (Florea, 1994) and solidifying metals (Zavaliangos and Anand, 1993; Martin et al., 1997).

The viscoplastic potentials are a way to generalize the stress and strain energy to viscoplastic materials. We know that the strain energy defined by the equation (2.18) can be introduced to define the relation between the stress and strain

$$\boldsymbol{\sigma} = \frac{\partial W}{\partial \boldsymbol{\varepsilon}}. \tag{2.40}$$

By components, that is

$$\sigma_{\xi\chi} = \frac{\partial W}{\partial \varepsilon_{\xi\chi}}. \tag{2.41}$$

Since the free energy depends on the physical configuration of the material, it is invariant to the stress and strain measure used to calculate it. By performing a Legendre transformation we can define a similar potential U that can be used to define the strain tensor

$$\boldsymbol{\varepsilon} = \frac{\partial U}{\partial \boldsymbol{\sigma}}, \tag{2.42}$$

where $U = \boldsymbol{\sigma} : \boldsymbol{\varepsilon} - W$. This gives us a connection $\boldsymbol{\varepsilon} = \boldsymbol{\varepsilon}(\boldsymbol{\sigma})$.

To generalize this kind of approach to plastic materials we need to introduce the concept of plastic history $\mathcal{H}$ (Lubarda, 2002). A set of variables ζ_j is used to describe the rearrangements of the material due to plastic deformations. These internal variables are used to describe the internal state of material, but not necessary in the usual way by the free energy being a point function of these variables. The free energy can also depend on the path by the way they were achieved. The plastic history of the material is the set of variables ζ_j along with their history, making it a functional of history of inelastic deformation. In the case of plasticity, both potentials defined in equations (2.40) and (2.42) should also depend on the plastic history $\mathcal{H}$. They give us an expression connecting the strain to stress $\boldsymbol{\varepsilon} = \boldsymbol{\varepsilon}(\boldsymbol{\sigma}, \mathcal{H})$ (and vice versa) at a given plastic history $\mathcal{H}$.

Using the concept of plastic history, we can define the plastic strain increment $\mathrm{d}^p\boldsymbol{\varepsilon}$ by

$$\mathrm{d}^p\boldsymbol{\varepsilon} = \boldsymbol{\varepsilon}(\boldsymbol{\sigma}, \mathcal{H} + \mathrm{d}\mathcal{H}) - \boldsymbol{\varepsilon}(\boldsymbol{\sigma}, \mathcal{H}). \tag{2.43}$$

This definition is illustrated in Figure 2.6. For plastic material, a change in plastic history can only be achieved by a stress loop which reaches the yield surface. Such a loop for one-dimensional case is illustrated in Figure 2.6. For one-dimensional problems, the loop is reduced to a line on stress axis. We start in point A with strain $\boldsymbol{\varepsilon}(\boldsymbol{\sigma}, \mathcal{H})$. We then increase stress and move in stress-strain space as determined by the stress-strain curve until we reach the point B. During this we gain plastic history variation $\mathrm{d}\mathcal{H}$, and increase stress by $\mathrm{d}\boldsymbol{\sigma}$. We see that the plastic strain increment is defined without any change in stress. We need to return to the same stress value as we have started with by moving from point B to point C, where strain is $\boldsymbol{\varepsilon}(\boldsymbol{\sigma}, \mathcal{H} + \mathrm{d}\mathcal{H})$, as required by the expression (2.43). This is achieved by elastic unloading, since we move away from the yield surface and the conditions for plastic deformation are no longer fulfilled. Keeping this stress path in mind we can express the plastic strain increment as

$$\mathrm{d}^p\boldsymbol{\varepsilon} = \mathrm{d}\boldsymbol{\varepsilon} - \mathsf{C} : \mathrm{d}\boldsymbol{\sigma}, \tag{2.44}$$

where C is the tensor of linear elastic moduli.

From the definition of potential U it is also clear that we can restate the plastic strain increment in terms of plastic increment of the potential

$$\mathrm{d}^p\boldsymbol{\varepsilon} = \frac{\partial U}{\partial \boldsymbol{\sigma}}(\boldsymbol{\sigma}, \mathcal{H} + \mathrm{d}\mathcal{H}) - \frac{\partial U}{\partial \boldsymbol{\sigma}}(\boldsymbol{\sigma}, \mathcal{H}) = \frac{\partial}{\partial \boldsymbol{\sigma}}\mathrm{d}^p U. \tag{2.45}$$

In this manner we have shown that there exists a potential for the plastic strain increment in a manner similar to the equation (2.42). This result will be used to show invariance of the viscoplastic potential on the frame of reference.

In viscoplasticity the governing equation of the viscoplastic strain rate is required, instead of an equation for the viscoplastic strain (Simo and Hughes, 1998). The equation for strain rate can be obtained by differentiating the equation (2.44) with respect to time t

$$\frac{\mathrm{d}^p\boldsymbol{\varepsilon}}{\mathrm{d}t} = \frac{\mathrm{d}\boldsymbol{\varepsilon}}{\mathrm{d}t} - \mathsf{C} : \frac{\mathrm{d}\boldsymbol{\sigma}}{\mathrm{d}t}. \tag{2.46}$$

The absence of the requirement to remain inside the yield surface gives us a straightforward way to design a viscoplastic potential. An infinitesimal change in stress is not any more accompanied by a change in strain but by

a change in strain rate. This means that we can devise a potential $\mathcal{U}(\boldsymbol{\sigma}, \mathcal{H})$ such that

$$\delta\boldsymbol{\sigma}\frac{\mathrm{d}^p\boldsymbol{\varepsilon}}{\mathrm{d}t} = \delta\mathcal{U} \tag{2.47}$$

and

$$\frac{\mathrm{d}^p\boldsymbol{\varepsilon}}{\mathrm{d}t} = \frac{\partial\mathcal{U}}{\partial\boldsymbol{\sigma}}. \tag{2.48}$$

Using the definition of plastic strain in the equation (2.45) we can see that

$$\delta\mathcal{U} = \frac{\delta\mathrm{d}^pU}{\mathrm{d}t}. \tag{2.49}$$

Since U is invariant on the choice of stress and strain measures so is $\mathcal{U}$. To formulate a viscoplastic model we only need to construct a viscoplastic potential, without any need for yield function or yield surface.

For example, we can try to construct viscoplastic potential for the toy-model studied in section 2.2.2. The viscoplastic strain rate is given by the equation (2.35) when $|\sigma| - \sigma_Y > 0$ and is equal to zero otherwise. This branching persists also in the definition of the viscoplastic potential

$$\mathcal{U} = \begin{cases} 0 & , \text{ if } |\sigma| - \sigma_y < 0 \\ \frac{1}{2\eta}\left(|\sigma| - \sigma_Y\right)^2 & , \text{otherwise.} \end{cases} \tag{2.50}$$

The definition of the potential with two branches is a consequence of the yield surface. The viscoplastic potentials, which do not try to mimic an existing yield surface model, are defined by a single branch but still in such a way that $\dot{\varepsilon}^p << 1$ when $|\sigma| < \sigma_0$ for some model-dependent critical stress σ_o.

2.2.4 Norton-Hoff model of viscoplasticity for metals

The viscoplastic potential theory described in the previous section can be used to devise models for many complicated viscoplastic materials. Such examples are soil (Kelln et al., 2008), concrete (Florea, 1994), crystals (François et al., 1998), biological tissue (Chen et al., 2013) and metals at high temperature (Zavaliangos and Anand, 1993) to name just a few.

The simplest and most widely used model to describe behavior of metals at high temperature is the Norton-Hoff model. It was first proposed for

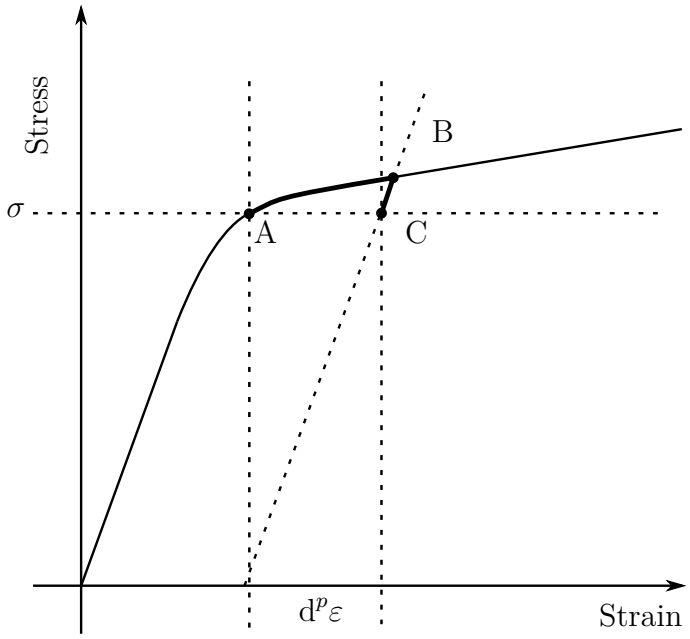

FIGURE 2.6: Illustration to the definition of plastic strain increment.

modeling high temperature creep of steel (Norton, 1929). The law has the following form

$$\dot{\boldsymbol{\varepsilon}}^p = \frac{3\boldsymbol{\tau}}{2\sigma_e}\varepsilon_0, \tag{2.51}$$

where ε_0 is given by

$$\varepsilon_0 = A \exp\left(-\frac{Q}{RT}\right)\left(\frac{\sigma_e}{\sigma_0}\right)^n. \tag{2.52}$$

In this equation the following quantities are used: the deviatoric stress $\boldsymbol{\tau}$ is given by $\boldsymbol{\tau} = \boldsymbol{\sigma} - \boldsymbol{I}\,\mathrm{tr}(\boldsymbol{\sigma})/3$. The effective stress σ_e is given by $\sigma_e = \sqrt{2\boldsymbol{\tau} : \boldsymbol{\tau}/3}$. R is the general gas constant and T is the absolute temperature. Q is experimentally determined activation energy. Also, the value of critical stress σ_0, the power n and constant A are material parameters determined by experiments.

The typical value of n for aluminium alloys is 4. This value falls neatly into the range 3-5, which indicates the so called "five-power-law creep". This name covers the laws of the form $\varepsilon_0 = A_o\sigma_e^n$, where $n \approx 5$. Such laws are usually valid for temperatures higher than half of the melting temperature (Kassner and Pérez-Prado, 2004). At lower temperatures, the power-law breakdown occurs and the value of Q decreases.

The driving mechanism for the "five-power-law creep" is dislocation climb and annihilation. The first theory of this was established by Weertman

(Weertman, 1955). It was based on prediction of annihilation rate of dislocations emanating from two dislocation sources. It predicted the power n to be between 3 and 5 depending on assumptions made in the model. Additionally, the model predicted correct activation energy. Experimentally, the values of Q in equation (2.52) were shown to be the same as for the self diffusion process, meaning that this process was limiting the rate of dislocation annihilation (Kassner and Pérez-Prado, 2004).

2.3 Hot tearing models

2.3.1 Hot tearing during DC casting of aluminium alloys

One of the most serious casting defects is hot tearing, the irreversible formation of a crack in the semisolid casting. The importance of hot tearing is reflected in many studies trying to understand various aspects of the phenomenon (Eskin et al., 2004a; Lalpoor et al., 2010) as well as in the development of numerical models to predict its occurrence (Hao et al., 2010; Farup and Mo, 2000; M'Hamdi et al., 2006; Sistaninia et al., 2013a).

To better understand the physical reasons for hot tearing, we should consider the solidification process of an aluminium alloy. Based on the permeability of the solid network, the process can be divided into four stages (adapted from (Eskin, 2008)).

1. *Mass feeding*, in which both, the already solidified dendrites and liquid melt are free to move.

2. *Interdendritic feeding*, in which the fluid has to flow through the already coherent solid skeleton.

3. *Interdendritic separation*, in which the liquid network becomes fragmented. With increasing solid fraction, liquid is isolated in pockets or immobilized by surface tension.

4. *Interdendritic bridging* or *solid feeding*, in which the billet has developed considerable strength and solid state creep compensates for further contraction.

Hot tearing usually occurs in the last two stages, in conditions, in which the liquid feeding is not sufficient to account for the shrinkage of the material. The shrinkage can be in general divided in two parts, the solidification shrinkage and thermal shrinkage. Thermal shrinkage is well known thermal isotropic contraction, while the reason for the solidification shrinkage is the difference in densities of solid and liquid phases. The thermal shrinkage is the main factor for stress occurrence in already solidified material while the solidification shrinkage is most relevant during the third stage of the solidification, when the liquid network becomes fragmented.

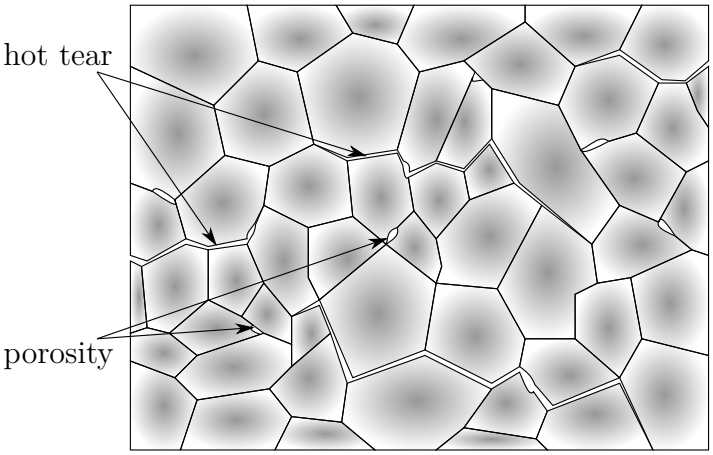

FIGURE 2.7: Illustration of cracks caused by hot tearing.

As a result of the shrinkage, stresses develop in the ingot. The existence of areas with tensile stress is one of the most important conditions for hot tearing. To the occurrence of hot tears is also facilitated by the fact that the yield stress decreases with increasing temperature. If the tensile stresses in an area increase over this value, the dendritic bridges that have formed collapse, initiating a hot tear.

The alloy composition is also an important factor determining the hot tearing probability. Different thermo-mechanical properties, different solidification range and variances in microstructure resulting from different chemical composition can make hot tearing even more difficult to predict (Eskin, 2008).

2.3.2 Lahaie-Bouchard model

The Lahaie-Bouchard (LB) model (Lahaie and Bouchard, 2001) is one of the many possible criteria for hot tearing. It describes the conditions under which the hot tearing can nucleate. It is one of the few stress-based criteria (Eskin and Katgerman, 2007). It formulates the rupture stress needed to separate two grains held together by liquid film.

The formulation of the model starts by stating the stress needed to separate two infinite beams bonded by capillary force due to a thin layer of liquid between them. The stress σ_c is given as

$$\sigma_c = \frac{2\gamma_l}{h}, \tag{2.53}$$

where γ_l is surface tension and h is the thickness of the liquid film. We notice that the σ_c decreases as h increases. This means, that if the critical stress is reached at a given thickness h, the two beams can be separated, since an increase in h will decrease the stress needed for further separation. If we replace the beams with a pair of grains, when this critical value of stress is exceeded a crack will start to grow.

The condition (2.53) that defines the critical stress for separation of two beams must be restated for a typical microstructure of the solidifying metal. To do this we consider an idealized cross-section of the mushy zone consisting of hexagonal solid grains separated by a thin layer of liquid as illustrated in Figure 2.8. The side of the hexagonal grains has length a and the thickness of the liquid film is h. We assume that once such a structure is subjected to uniaxial stress, the strain in the direction of stress $\varepsilon_{\parallel}$ is accumulated only by the change of the liquid layer thickness without any deformation of grains. This gives us

$$\varepsilon_{\parallel} = \frac{h - h_0}{\sqrt{3}a}, \tag{2.54}$$

where h_0 is the thickness of liquid layer in the unstrained configuration. This thickness is connected to the solid fraction f_s by the following formula (Lahaie and Bouchard, 2001)

$$h_0 = \sqrt{3}a\frac{1 - f_s^m}{f_s^m}. \tag{2.55}$$

The power m is determined by the microstructure. If the microstructure is columnar, the value $m = 1/2$ is used and if the microstructure is equiaxed

the value is $m = 1/3$. The size of the solid grains a can be calculated from the grain size d_g by equating areas of a hexagon with side a to the area of circle with radius d_g. Combining all this to express the film thickness h in equation (2.53) gives the following critical stress

$$\sigma_{LB} = \frac{4}{3\sqrt{\frac{\pi}{\sqrt{2}}}} \frac{\gamma}{d_g \left(\frac{1-f_s^m}{f_s^m} - \varepsilon_{\|}\right)}. \tag{2.56}$$

Hot tearing can start when stress is larger than σ_{LB}. The stress to which we compare this value is simple to define in quasi one-dimensional setting which is used to construct this equation, but in general three-dimensional setting we need to be more careful. The hot-cracking susceptibility (HCS) can than be defined as

$$HCS = \frac{\sigma_{max}}{\sigma_{LB}}. \tag{2.57}$$

The value σ_{max} is the maximum principal stress. In the definition of the critical stress the strain was defined in the same direction as the stress. This means that the strain, which is used in the critical stress formula, is the strain in the direction of maximal principal stress $\varepsilon_{\|} = \boldsymbol{n}_{max}^T \boldsymbol{\varepsilon} \boldsymbol{n}_{max}$, where $\boldsymbol{n}_{max}$ is the direction of maximal principal stress.

2.3.3 Suyitno-Kool-Katgerman model

The Suyitno-Kool-Katgerman (SKK) model belongs to a class of more sophisticated two-phase models. Besides providing us with a condition for occurrence of hot tearing it also provides a model for microporosity. It is more sophisticated than the rest of the models since it was developed especially for the needs of numerical modeling (Suyitno et al., 2009). Because of this, it includes variables which are impossible to measure reliably but are easily provided by numerical models.

The models starts by stating the conservation equation for three phases, each associated with a volume fraction.

$$f_s + f_l + f_v = 1, \tag{2.58}$$

where f_s is solid fraction, f_l is liquid fraction and f_v is volume fraction of voids. Mass conservation for a control volume gives us a rate equation for void fraction

$$\dot{f}_v = \dot{f}_r + \dot{f}_e, \tag{2.59}$$

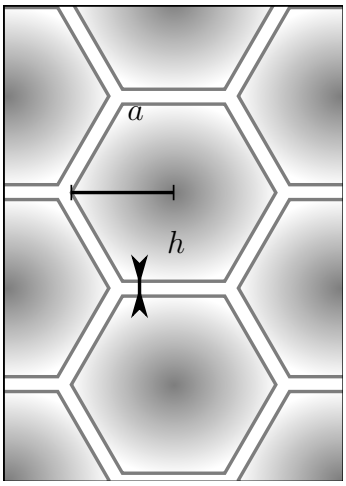

FIGURE 2.8: The microstructure cross-section used for formulation of LB model. The gray hexagons represent the solid grains and the white channels the liquid film between them.

where $\dot{f}_r$ is the shrinkage rate and $\dot{f}_e$ is the feeding rate. The model states that the voids start to nucleate when $\dot{f}_r - |\dot{f}_e| > \dot{f}_c$. The parameter $\dot{f}_c$ is the critical rate for void nucleation. It is material dependent but very small, so $\dot{f}_c = 0$ can be used instead of its actual value.

The shrinkage rate takes into account solidification shrinkage and material deformation

$$\dot{f}_r = -\left(\frac{\rho_s}{\rho_l} - 1\right)\dot{f}_l + \frac{\rho_s}{\rho_l} f_s \mathrm{tr}\left(\dot{\boldsymbol{\varepsilon}}\right). \tag{2.60}$$

The feeding term accounts for the liquid feeding of the melt. In the coherent part of the mushy zone the liquid has to flow through a solidified network of dendrites. Such a flow can be described by Darcy law. Combining this with Caraman-Kozeny relation, which is the standard model to calculate permeability of the mushy zone from the solid fraction (Eskin, 2008), we obtain the following expression for the feeding term

$$\dot{f}_e = \nabla \cdot \left(\frac{d_{as}^2}{180\eta} \frac{f_l^3}{1 - f_l} \nabla p\right). \tag{2.61}$$

The permeability of the mush is determined by the dendrite arm spacing

d_{as} and the viscosity of the melt η. The driving therm is the gradient of the pressure p.

In the locations, where the condition for cavity growth is fulfilled, the void formation rate can be integrated to obtain the fraction of voids. Assuming spherical voids, their diameter is given by

$$a = \left(\frac{3}{2\pi} C d_g^3 f_v\right)^{1/3}. \tag{2.62}$$

Here d_g is the grain diameter and C packing parameter, which depends on the packing of the grains. If the grains are packed in bcc lattice the parameter has value $C = 8/(3\sqrt{3})$. Knowing the size of the voids in the material can be used to determine the critical stress needed for crack growth σ_{SKK}. For this we can use the result from Griffith theory of brittle fracture which connects the diameter of a void with critical tensile stress needed for a crack to nucleate on the void

$$\sigma_{SKK} = \sqrt{\frac{4\gamma_s E}{\pi a}}. \tag{2.63}$$

The only additional parameter in this equation is the surface energy γ_s. In the same manner as in the case of LB model we can use the criterion

$$HCS = \frac{\sigma_{max}}{\sigma_{SKK}} \tag{2.64}$$

to describe the hot tearing susceptibility of the material.